

# Grain Boundary Resistance in Copper Interconnects from an Atomistic Model to a Neural Network

Daniel Valencia\* and Evan Wilson

*Birck Nanotechnology Center, Network for Computational Technology,  
Purdue University, West Lafayette, 47907, USA*

Zhengping Jiang

*Samsung Semiconductor Inc, San Jose CA, 95134, USA*

Gustavo A. Valencia-Zapata, Gerhard Klimeck, and Michael Povolotskyi

*Birck Nanotechnology Center, Network for Computational Technology,  
Purdue University, West Lafayette, 47907, USA*

## Abstract

Orientation effects on the specific resistance of copper grain boundaries are studied systematically with two different atomistic tight binding methods. A methodology is developed to model the specific resistance of grain boundaries in the ballistic limit using the Embedded Atom Model, tight binding methods and non-equilibrium Green's functions (NEGF). The methodology is validated against first principles calculations for thin films with a single coincident grain boundary, with 6.4% deviation in the specific resistance. A statistical ensemble of 600 large, random structures with grains is studied. For structures with three grains, it is found that the distribution of specific resistances is close to normal. Finally, a compact model for grain boundary specific resistance is constructed based on a neural network.

---

\* valencid@purdue.edu

## I. INTRODUCTION

Due to the aggressive downscaling of logic devices, interconnects have reached the nanoscale, making quantum effects important. According to the roadmap provided by ITRS, interconnects are expected to reach sizes of 10 to 30 nm in the next decade [1]. Previous work by Graham et al. [2] demonstrates that surface scattering and grain boundary (GB) scattering play major roles in the resistance of structures smaller than 50 nm. Earlier works based on semi-empirical parameters have described polycrystalline films and surface scattering [3, 4] for macroscopic systems, but the fact that those models require fitting parameters for each experimental setup limits the scope of their applications. The ultra-scaled interconnects suggested by the roadmap require better descriptions of orientation and confinement effects to correctly model scattering in wires. Recently, first-principles calculations have been used to describe the resistance of a single grain boundary by making use of non-equilibrium Green's function with Density Functional Theory (DFT-NEGF) formalism [5]. The results demonstrate a strong correlation between resistance and the geometry of the grain boundary, and show agreement with both experimental [6] and other theoretical work [7–9]. However, the studied structures are limited to relatively small sizes containing single grain boundaries and less than a few hundred atoms because of the computational burden required to perform DFT-NEGF calculations.

The purpose of this manuscript is to introduce an atomistic model that describes the resistivity due to grain boundary effects for realistic copper interconnects as projected by the ITRS roadmap [1] without depending on any phenomenological parameter. Even though the atomistic model is much faster than an *ab initio* method, parametric models have the advantage of easily providing a quantitative value of resistivity. Therefore, a compact model which reduces the computation time is generated by making use of a neural network that is based on large statistical sample. The rest of the manuscript has been organized as follows. Section II presents the main characteristics of the atomistic models and benchmarks tight binding parameters against first principles calculations for a copper FCC structure. Section III constructs single grain boundaries based on coincident site lattice (CSL) and validates their electronic properties against an *ab initio* method. Section IV describes grain boundary effects on copper interconnects using a system of three grains of 10 nm length simulated with an atomistic method which is benchmarked in the previous sections and quantifies

the effect of misorientation. Section V proposes a compact model based on three different algorithms and finds that a neural network approach best matches the results obtained from the atomistic methods, allowing the results to be generalized to any grain boundary system configuration with a total length of 30 nm. Section VI presents a summary of this work.

## II. DESCRIPTION OF TIGHT BINDING MODELS

The two tight binding methods used in this study are an environmental orthogonal tight binding model (TB) [10] and a non-orthogonal tight binding method based on the Extended Hückel (EH) model [11]. The TB model has an orthogonal basis with an interaction radius up to the second nearest neighbor (2NN). However, it requires a large number of parameters to include strain effects (48 parameters for copper). In comparison, the EH model has a non-orthogonal basis with a larger interaction radius up to the third nearest neighbor (3NN). It requires a smaller number of parameters than the TB method (11 parameters for copper).

Existing parameters for the TB model [10] fail when used in highly distorted atomic systems such as GB. Due to the exponential dependence of the inter-atomic coupling on the bond length, the inter-atomic matrix elements corresponding to bond lengths with a 5% or greater distortion generate unphysical results. The problem is solved by obtaining a new parametrization with additional constraints on the inter-atomic coupling. This new parameter set is summarized in TABLE VIA in Appendix A. The parameters for the EH model are taken from literature [12]. Both EH parameters and the new TB parameters show a good match for the Cu unit cell when compared against an *ab initio* method as shown in Fig. 1. The *ab initio* result, used as a reference, is obtained by density functional method with a Perdew-Burke-Ernzerhof version of the generalized gradient approximation (GGA PBE) exchange- correlation functional [13]. An energy cutoff of 150 Ry is used and the Brillouin zone is sampled with a  $10 \times 10 \times 10$  mesh. An FCC copper lattice with a lattice constant of 0.361 nm, as reported experimentally [14], is considered.

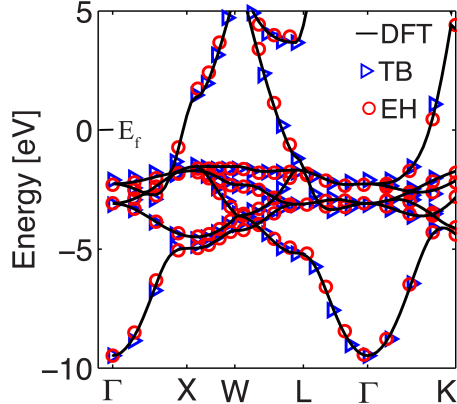


FIG. 1. Band structure for copper unit cell obtained by TB, EH and DFT methods.  $E_f$  indicates the Fermi energy.

### III. COINCIDENT SITE LATTICE GRAIN BOUNDARIES

To validate the tight binding models, the effects of GB scattering were studied for a single coincident site lattice grain boundary. The simplest GB configurations are obtained by a rotation of one of the grains until its lattice vector becomes coincident with the vector of the unrotated lattice [15] as shown in Fig. 2. A fairly small number of atoms ( $< 400$ ) is required to construct these systems, which allows the tight binding models to be benchmarked against a first principles calculation as implemented in the ATK package [13].

CSLs are labeled by  $\Sigma N$ , where  $N$  corresponds to the ratio of the CSL unit cell size to the standard unit cell size. In this work, the CSL GB are generated with GBSTUDIO [16] and relaxed using an *ab initio* method. The relaxation is carried out with GGA PBE exchange-correlation functional. A Double Zeta polarized basis set is used for copper atoms with an energy cutoff is 150 Ry and the Brillouin zone sampled with a  $4 \times 4 \times 1$  mesh, until all atomic forces on each ion are less than  $10^{-5}$  eV/Å. Once the ionic relaxation is completed, the transmission spectrum for CSL structures is calculated by the recursive Green's function method [17] implemented in NEMO5 [18] in an energy range between -2 and 2 eV around the Fermi level with a Brillouin zone sampled with a  $30 \times 30 \times 1$  mesh.

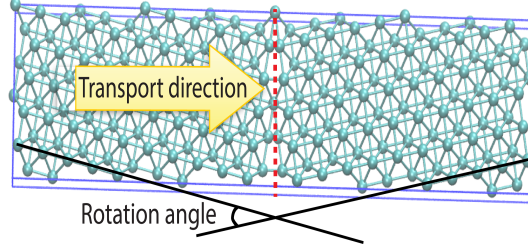


FIG. 2. Coincident site lattice GB are obtained by generating a superposition of two periodic lattices. One of the lattices was rotated with respect to the other, generating coincident points between the lattices for each rotation angle.

The integrated transmission spectra in the  $k$  space obtained by the tight binding methods are compared against the spectrum obtained by the *ab initio* method with a similar basis set, energy cutoff and Brillouin mesh as is used in the ionic relaxation. The results in Fig. 3 show that the EH method captures the main features of DFT not only at the Fermi energy ( $E_f$ ), but also over a large energy window. On other hand, while the transmission spectrum calculated by TB also shows reasonable agreement with DFT around the Fermi window, it fails to describe the *ab initio* transmission spectrum for energies away from the  $E_f$ .

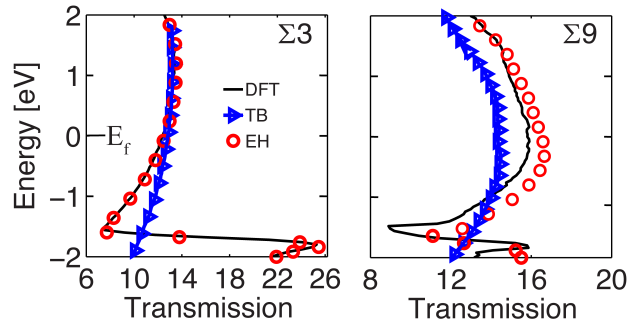


FIG. 3. Transmission spectra  $T(E)$  for two different CSL ( $\Sigma 3$  and  $\Sigma 9$ ) show that EH captures the main features of DFT.

Subsequently, the resistance for the CSL GB in the ballistic limit is obtained based on the Landauer formalism assuming a low bias condition [19] as:

$$G = \frac{1}{R} = \frac{2e^2}{h} \int T(E_f, \mathbf{k}) d^2k, \quad (1)$$

where  $G$  is the conductance,  $R$  is the resistance,  $e$  is the elementary charge,  $h$  is Planck's constant and  $T(E_f, \mathbf{k})$  is the transmission for a particular wave vector  $\mathbf{k}$  at the Fermi energy.

The Fermi levels in Figs. 1 and 3 are calculated at the leads of the device self consistently for DFT and non-self consistently for tight binding models. In this last case, the Fermi level is obtained by integrating over the DOS from  $-\infty$  to  $E_f$  until this value becomes equal to the total number of electrons at a zero temperature approximation [20]. Following Ref. [5] the specific resistances of the CSL grain boundaries are obtained by  $\gamma^R = (R - R_B) A$ , where  $R$  is the resistance of the configuration that contains the GB,  $R_B$  is the resistance of the perfect bulk copper, and  $A$  is the grain cross section. The specific resistances for those CSL configurations are calculated by TB and EH and compared to DFT as shown in Table I

CSL GB	Specific resistance CSL $\gamma^R$ ( $10^{-12}\Omega cm^2$ )				
	$\gamma_{DFT}$	$\gamma_{EH}$	$\gamma_{TB}$	Experimental	Other References
$\Sigma 3$	0.156	0.173	0.158	0.170 [21]	0.202 [6]
					0.155 [8]
					0.158 [5]
					0.148 [9]
$\Sigma 5$	1.759	1.934	2.240		1.885 [6]
					1.49 [5]
$\Sigma 9$	1.82	1.72	2.14		1.75 [5]
$\Sigma 11$	0.64	0.57	0.71		0.75 [5]
$\Sigma 13$	2.01	1.72	2.09		2.41 [5]

TABLE I. Specific resistance for different CSL ( $\Sigma N$ ) calculated by TB, EH and DFT.

The results in the Table I and Fig. 4 show less than 10.4 % difference in the specific resistance between EH and DFT, and less than 11.2% between TB and DFT. Thus the atomistic methods (TB and EH) are able to describe copper interconnects with reasonable accuracy. These methods are chosen to study GB systems with  $10^3$  to  $10^4$  atoms because they require significantly fewer computer resources than the *ab initio* calculations [20].

Only non *ab initio* methods are capable of relaxing structures of this size ( $\gg 10^3$  atoms), therefore a force field potential method based on an Embedded Atom Model (EAM) is used. The relaxation is performed using LAMMPS software package [22] with an EAM potential constructed by Y. Mishin et al. that is fitted to first principles calculations to correctly describe grain boundaries and point defects in copper [23]. .

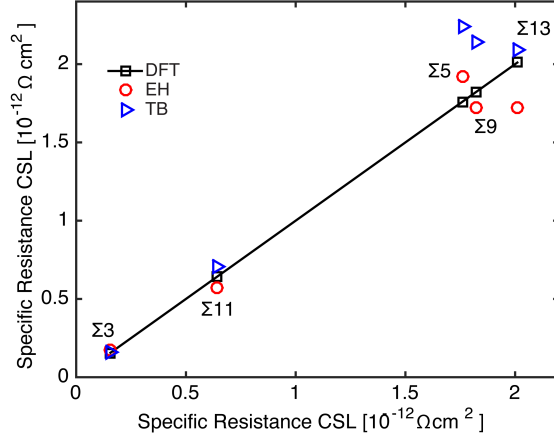


FIG. 4. Resistivities for different CSLs, labeled by  $\Sigma N$ , calculated by TB and EH and compared with the DFT method.

The accuracy of this approach is determined by comparing the formation energy for CSL GBs obtained by *ab initio* and the EAM method. The formation energy  $\gamma^E$  is defined as follows:

$$\gamma^E = \frac{E_{slab} - NE_0}{A}, \quad (2)$$

where  $E_{slab}$  is the total energy of a slab configuration that contain a CSL GB,  $N$  is the number of atoms in the CSL GB,  $E_0$  is the energy of a single atom of bulk copper and  $A$  the cross sectional area. The ionic relaxation carried out by *ab initio* methods used the plane wave DFT package (VASP) [24] and a PBE GGA exchange-correlation functional. The plane wave energy cutoff is 500 eV and the Brillouin zone is sampled with a  $4 \times 4 \times 1$  mesh, until all atomic forces on each ion are less than  $10^{-5}$  eV/Å. Comparison of the relaxation energy, computed using the EAM potential, with the DFT result (see Fig. 5), shows that the difference is less than 7% with for all CSL orientations except the  $\Sigma_{11}$ , which shows a larger error of 20 %. These results indicate that the EAM potential calculation is an acceptable method to relax the grain boundary structures with the benefit of reduced computational burden, compared to DFT.

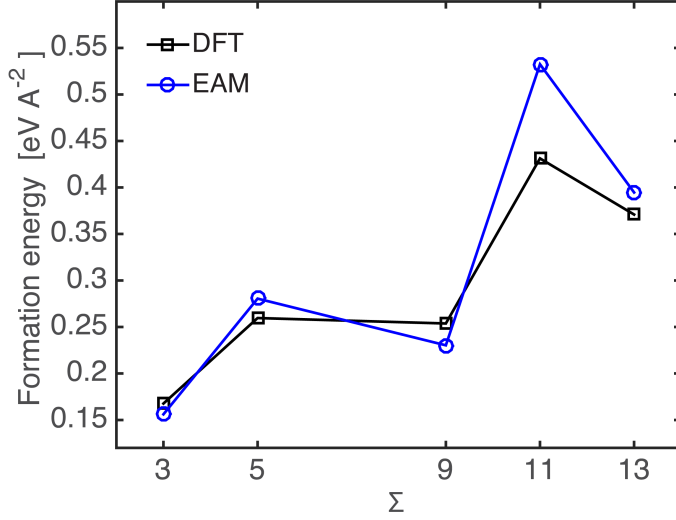


FIG. 5. Formation energy ( $\gamma^E$ ) for different CSLs GB, labeled by  $\Sigma N$ , relaxed by DFT and EAM potential.

#### IV. SPECIFIC RESISTANCE FOR GRAINS OF 10 NM LENGTH

Based on the prediction of the ITRS roadmap that interconnects will reach 10 to 30 nm length in the coming years [1], a set of copper thin films of 30 nm is constructed and modeled by tight binding methods as described in Section II. The copper interconnects are formed by three grains of 10 nm length. Each grain is constructed with a super cell growing in the [110] orientation with a lattice constant of 0.361 nm which has the highest conductance [10], as reported experimentally [14]. In order to quantify the effect of GB orientation on the specific resistances for copper interconnects, two different types of GBs are generated by Voronoi diagrams [25]. These GB types are based on the rotation direction of the middle grain shown as “Tilt” and “Twist” GBs respectively, which generates two boundaries as shown in Fig. 6 a) and b). In order to have a lower impact on the specific resistivity due to the electrode setup, three grains are modeled in this work. In both configurations, only the middle GB is initially rotated then a periodic boundary condition is applied in the [001] direction for the ionic relaxation and the electronic transport calculation. Therefore, atomic surface roughness is present in the structures as a result of the relaxation. Additionally it is assumed that each configuration shown in the Fig. 6 and 8 is connected to a pristine source and drain lead oriented in the [110] direction, whose atoms are fixed during the ionic



relaxation.

The “Tilt” GBs are generated by a rotation of the middle grain with respect to the  $[001]$  direction by an angle  $\theta$  in a range between 0 and  $\pi/2$ . Each grain is formed by a supercell of 10 nm length ( $L$ ) in the transport direction  $[110]$ , 10 nm width ( $W$ ) in the  $[\bar{1}01]$  direction and 0.361 nm thickness ( $T$ ) in the periodic direction  $[001]$  as shown in Fig. 6 a) and c).

The “Twist” GBs are generated by a rotation of the middle grain with respect to the  $[\bar{1}11]$  direction by an angle  $\theta$  in a range between 0 and  $\pi/2$ . The rotation is applied in the same direction as the periodicity, therefore thicker grains are constructed to ensure the grains overlap after rotation. In this configuration setup each grain is formed by a supercell of 10 nm length ( $L$ ) in the transport direction  $[110]$ , 3 nm width ( $W$ ) in the  $[\bar{1}01]$  direction and 3 nm thickness ( $T$ ) in the periodic direction  $[001]$  as shown in Fig. 6 b) and d).

It is important to clarify that after any rotation for “Tilt” or “Twist” GB the  $[110]$  direction is no longer the transport direction for that grain. Similarly, the rotation angle corresponds to the initial value, but this value will be slightly modified after relaxing the structure.

The specific resistance for “Tilt” and “Twist” GBs for different orientations are obtained by a procedure similar to that described in Section III as  $\rho = R \times A$ , where  $R$  is obtained by Eq. (1) and each configuration is relaxed by an EAM potential. In order to compare the specific resistivity for “Tilt” and “Twist” GBs for different angles  $\theta$ , the “Tilt” GBs values are normalized such that “Tilt” and “Twist” GBs are calculated over the same cross sectional area. Those values are plotted in Fig. 7. In both systems, specific resistance increases with an increase in the angle, until the angle reaches  $\pi/6$ , and then becomes almost constant, although the “Tilt” GB shows a reduction after  $\pi/3$ . The specific resistance dependence for “Twist” GBs shows more noise than for “Tilt” GBs, because “Twist” structure has more points per unit area where the grain boundaries intersect (see Figs. 6c, d), which leads to a higher number of dislocations. Differences between TB and EH, especially pronounced for “Twist” GBs, are due to the fact that the TB model does not correctly describe strained systems, where the atoms are coupled by distances much smaller than the bulk bond length. In particular, for the “Twist” system with rotation angles such as 6, 8 and 70 degrees, there are many atoms with a small distance between nearest neighbors which results in

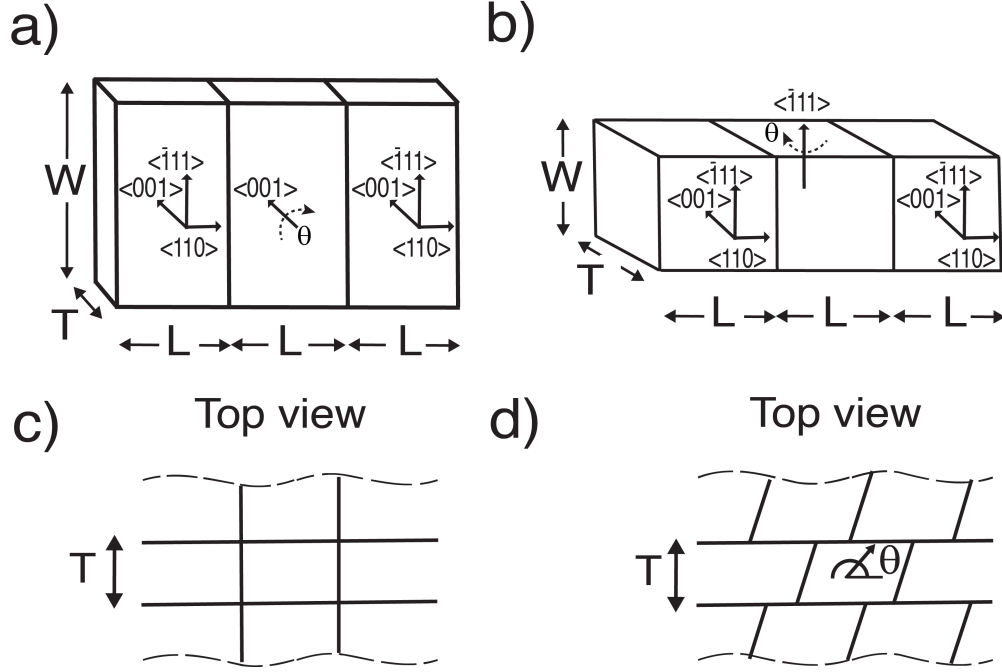


FIG. 6. GB classification: a) “Tilt” GB are generated by a rotation in the  $[001]$  plane b) “Twist” GB generated by a rotation in the  $[\bar{1}01]$  plane where the grain boundary is always perpendicular to the transport direction. c) and d) figures represent the top view of “Tilt” and “Twist” GB configurations.

unphysical peaks in the specific resistance dependence (see Fig. 7b) when it is calculated by the TB method.

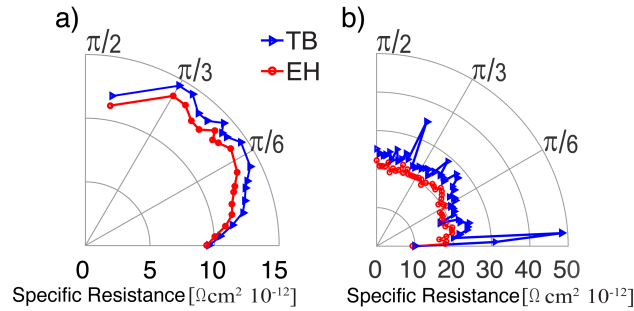


FIG. 7. a) “Tilt” and b) “Twist” GB specific resistance calculated by the TB and EH methods.

In order to understand and create a compact model to predict how specific resistance changes as a result of GB orientation, a sample set of 600 configurations are generated. Each GB is constructed with three grains and each of them is rotated with an angle  $(\alpha, \beta, \gamma)$  in a

range between 0 to 180 degrees parallel to the GB boundary. The dimensions of the GB are similar to those used for “Tilt” GB with thickness, width and length equal to 0.5 nm, 3 nm and 10 nm respectively as shown in Fig. 8. A periodic boundary condition in the  $[001]$  direction is imposed.

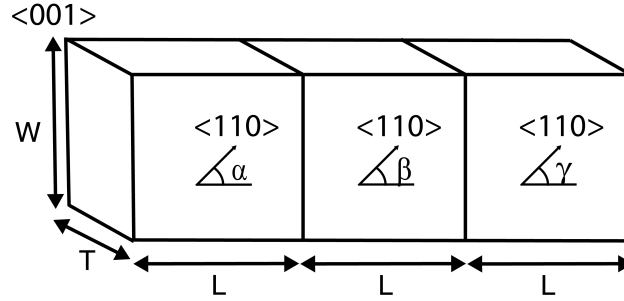


FIG. 8. GB configuration constructed with three grains, each one generated by rotating the lattice through angles  $\alpha, \beta, \gamma$ , respectively, around the  $[001]$  axis.

The specific resistance for these samples is calculated with the EH method because it is more reliable over angle rotations than the TB method. Making use of the results obtained from these samples, a boxplot for  $\alpha$  and  $\gamma$  in a range between 0 to 180 degrees and a constant angle  $\beta$  is plotted in Fig. 9 which shows a symmetry in the specific resistance in a range between 0 to 90 degrees and 90 to 180 degrees. This observation is confirmed by a statistic nonparametric Kolmogorov-Smirnov test [26] which compares the distribution function for the group of samples in a range between 0 to 90 degrees against those between 90 to 180 degrees and finds that both groups of samples are drawn from an equivalent, continuous distribution. A p-value of 0.16 is obtained for the Kolmogorov-Smirnov test, confirming that there is no difference between the specific resistance distributions for both cases with a confidence of 95%. The symmetry in the specific resistance is due to the fact that the crystal symmetry of copper is not totally disrupted by the structural relaxation. The probability distribution for the three different angles ( $\alpha, \beta$  and  $\gamma$ ) in a range between 90 to 180 degrees is plotted in Fig. 10. Per the Shapiro-Wilk test [26] with a p value of 0.15 and a 95% confidence, the specific resistance distribution follows a normal distribution with a mean and standard deviation equal to  $31.7 \times 10^{-12} \Omega cm^2$  and  $2.8 \times 10^{-12} \Omega cm^2$ . The Q-Q plot in Fig. 10 b) shows that the specific resistance distribution is likely normal, although the left and right tails do not follow a normal distribution.

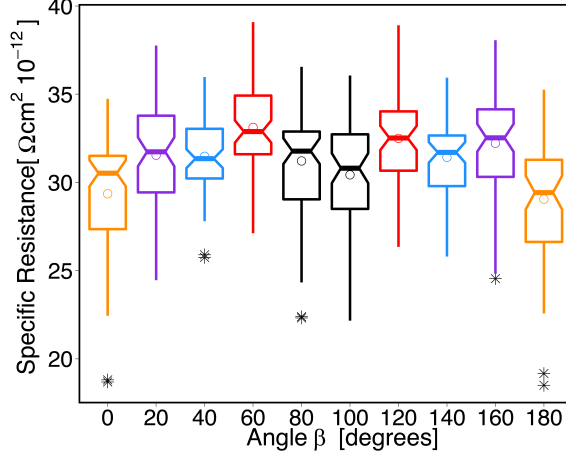


FIG. 9. Resistivity distributions for  $\alpha$  and  $\gamma$  between 0 to 180 degrees and a constant angle  $\beta$ . The boxplots represent the resistance distribution, while those marked with a star represent outliers.

## V. GRAIN BOUNDARIES MODELED BY A NEURAL NETWORK

Atomistic models based on a tight binding approach can describe the effects of the GB orientation on specific resistance with the same accuracy as DFT methods, but with a much lower computational burden. However, the specific resistance calculated by atomistic models such as EH and TB for a combination of three grains of 10 nm length in the transport direction are still not as fast as conventional models such as the Fuchs-Sondheimer and Mayadas-Shatzkes models [3, 4] which describe surface roughness and grain boundary effects respectively in copper interconnects. However these models require experimental input to fit some parameters which limits the transferability for different configurations. Therefore, compact models based on the statistical results obtained from an atomistic model described in Section IV are proposed to describe the scattering effects on grain boundaries for a system of 3 grains of 10 nm length. Three different algorithms are used to construct the compact models, including a polynomial fit, a nearest neighbor search model and a neural network as described in the following subsections. The inputs for the compact models are the orientation angles  $\alpha$ ,  $\beta$  and  $\gamma$  and the output is the specific resistance of the GB  $\rho(\alpha, \beta, \gamma)$ . The compact models are trained with a random selection of 80% of the 600 samples plotted in the Fig. 10 and validated with the remaining 20% of the data.

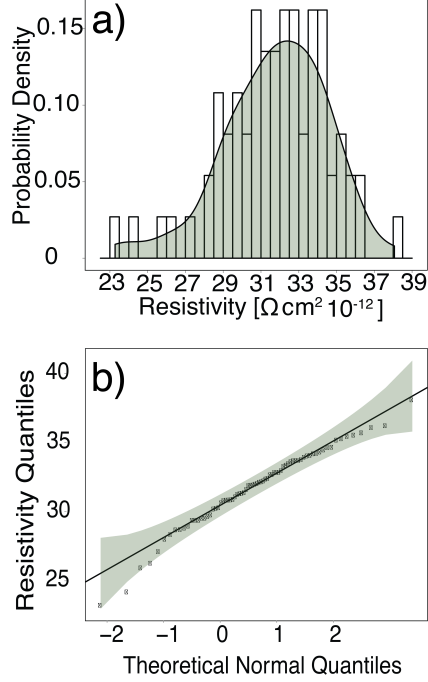


FIG. 10. a) Probability distribution for a GB system rotated over three different angles  $\alpha$ ,  $\beta$  and  $\gamma$  in a range between 90 and 180 degrees. The shaded area represents the best approximation of a normal distribution for the 600 samples; b) Q-Q plot which confirms the normal distribution.

### Polynomial Fit

A polynomial fit of second order is carried out based on a least squares adjustment, obtaining the following parametric relationship between the misorientation angles ( $\alpha, \beta, \gamma$ ) and the specific resistivity:

$$\begin{aligned} \rho(\alpha, \beta, \gamma) = & 21.95 + 10.59\alpha - 2.76\alpha^3 + 10.54\beta \\ & - 6.15\beta^2 + 13.41\gamma - 3.91\beta\gamma - 5.18\gamma^2 \end{aligned} \quad (3)$$

The expected values obtained from the model are compared against the remaining 20% of the atomistic data as show in the figure 11. The parametric fitting based on a polynomial approximation displays a poor match with the atomistic results with a 70% variability of

the resistivity for the training dataset and a MSE equal to  $13.94 \times 10^{-12} \Omega cm^2$ . This result shows that grain boundary effects cannot be modeled as a simple additive effect between each orientation. Therefore, a more complicated dependency exists between the resistivity and the orientation angles.

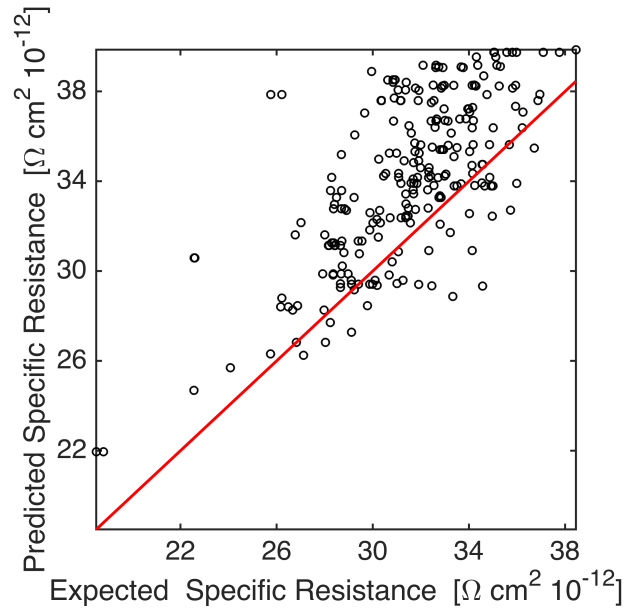


FIG. 11. Evaluation of the specific resistance for the multivariate polynomial model using least squares adjustment for the remaining 20% of  $\rho(\alpha, \beta, \gamma)$  values for copper interconnects.

### Nearest Neighbor Fitting

Since the polynomial fit provides a poor fitting for the specific resistance of a GB oriented by the angles  $(\alpha, \beta, \gamma)$ , a non-parametric model is explored based on a “Nearest-Neighbor” search which uses the “dsearchn” triangulation method implemented in Matlab’s optimization package [27]. The comparison between the expected specific resistance and the predicted specific resistance obtained from the testing data is plotted in Fig. 12. While this algorithm exhibits a mean square error for the specific resistance equal to  $2.67 \times 10^{-12} \Omega cm^2$  which is much lower than the error of the polynomial method, it does not support systems that have more than 3 degrees of freedom.

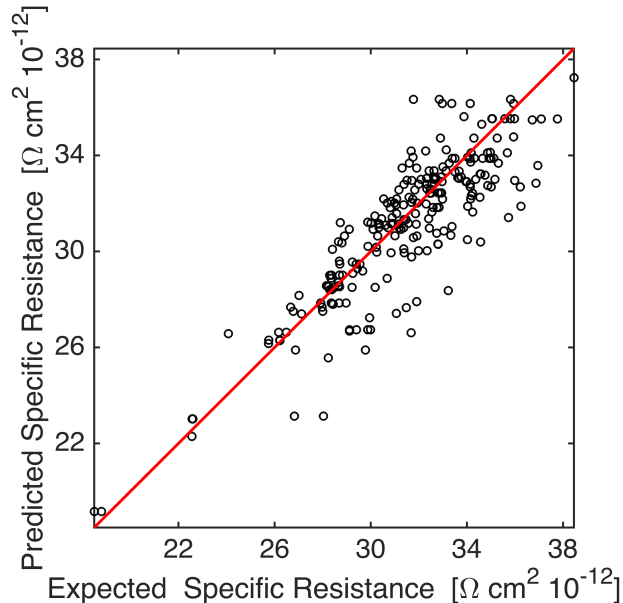


FIG. 12. Evaluation of the specific resistance for the Nearest Neighbor model for the remaining 20% of  $\rho(\alpha, \beta, \gamma)$  values for copper interconnects.

### Neural Network Model

Finally, a compact model based on a Neural Network (NN) [28] algorithm is introduced. NN models have been widely used to model complex problems; in the TB approach, NN algorithms have been used to describe potential minimization [29] and materials parametrization [30]. In this work, a multilayer neuronal network (MLN) is applied with a back-propagation algorithm [28] to quickly obtain the specific resistance of the GB. .

The neural network shown in Fig. 13 is achieved after testing different types of neural networks and varying the number of hidden layers. The final system is formed by an input layer, three hidden layers, and one output layer. The input layer  $\mathbf{p} = (\alpha, \beta, \gamma)$  is represented by a row vector of dimension  $3 \times 1$ . The hidden layer is composed of three inner layers  $i$  with 10, 6, and 3 neurons, respectively; the weight  $\mathbf{W}^i$  and bias  $\mathbf{b}^i$  vectors for a given layer  $i$  are shown in Fig. 13.

The MLN is implemented in the statistical software R making use of the package Neuralnet [31]. The value of the parameters  $\mathbf{W}^i$  and bias  $\mathbf{b}^i$  are obtained by the gradient descent method [32] which minimizes the mean square error of the output layer. In the NN, the

functions  $f^i$  represent logistic functions employed at each layer, except for the last layer  $f^4$  to which is applied a linear function.

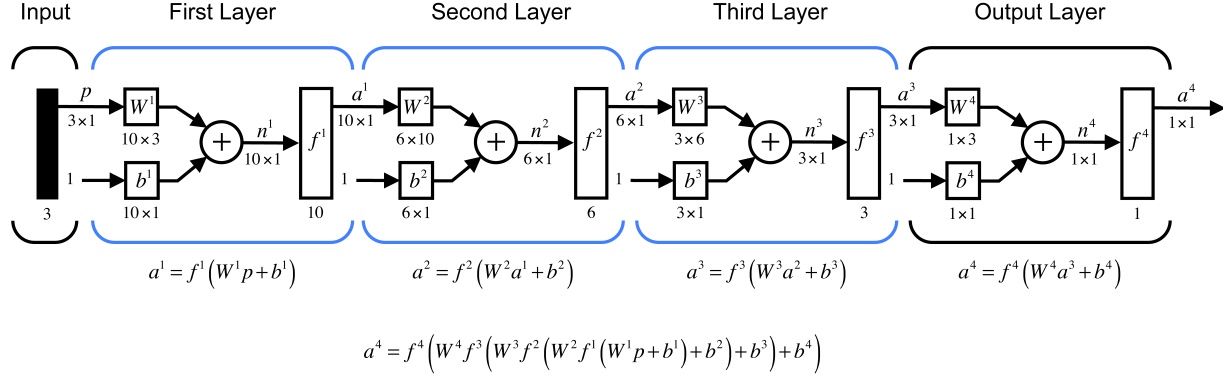


FIG. 13. Schematic representation for the Multi-Layer Neural Network used to describe grain boundary specific resistance for copper interconnects with three grains. The values  $W^i$  and  $b^i$  correspond to the weights and bias parameters,  $f^i$  represents logistic functions except for the last layer  $f^4$  to which is applied a linear function and  $a^i$  corresponds to the output at each neuron  $i$ .

The mean square error (MSE) prediction for specific resistance for this NN is  $1.44 \times 10^{-12} \Omega \text{ cm}^2$ . The results obtained for the testing data of the MLN are plotted in Fig. 14; the model shows good agreement for low values of specific resistance and larger variability for GB with a specific resistance over the range  $29.0 - 39.0 \times 10^{-12} \Omega \text{ cm}^2$ .

Comparing the three methods described above, it is observed that the neural network method has a much smaller MSE than the other methods. It can also be generalized to describe more complicated configurations with different geometries and a number of grains not possible with non-parametric methods such as “Nearest Neighbor” or linear fitting.

## VI. SUMMARY

In summary, the effect of orientation on grain boundary resistance for copper interconnects is studied using two different atomistic tight binding methods (EH and TB). The transmission spectrum and specific resistance calculated by these methods are benchmarked for coincident site lattice single GB ( $\Sigma N$ ) against first principles calculations. These results show that the EH method captures the main features of DFT in the Fermi window between



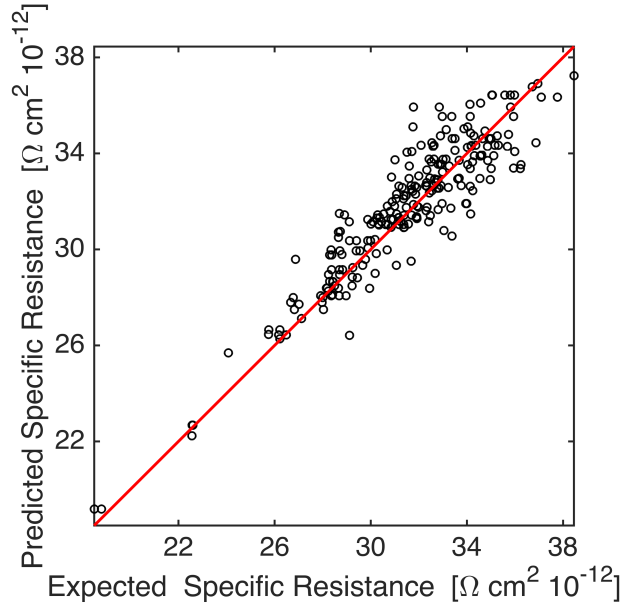


FIG. 14. Evaluation of the specific resistance for the Multi-Layer Neural Network model for the remaining 20% of  $\rho(\alpha, \beta, \gamma)$  values for copper interconnects.

-2 to 2 eV. On other hand, the transmission spectrum calculated by TB also shows reasonable agreement with DFT around the Fermi window, but fails to describe the *ab initio* transmission spectrum for energies away from the Fermi energy. Since the computational requirements for tight binding methods are also much smaller than for first principle calculations, the EH method is an effective way to describe the specific resistance of interconnects with lengths greater than 30 nm.

Orientation effects for “Tilt” and “Twist” GBs for copper interconnects of 30 nm length relaxed by a semi-classical EAM potential are also benchmarked against first principles. Rotations perpendicular to the transport direction have a larger effect on the specific resistance of the GB than rotations parallel to the transport direction. Statistical analysis of GB specific resistance shows that the inversion symmetry of copper is still manifested for the considered grain geometry.

Finally, statistical models based on three different algorithms are studied. The parametric model based on a polynomial fit of the misorientation angles  $(\alpha, \beta, \gamma)$  shows a poor match with the test results from the atomistic model, confirming that a complex relationship exists between the specific resistance and the orientation angles. While the nearest neighbor model displays a better fit with an error of  $2.67 \times 10^{-12} \Omega cm^2$ , it can only support three degrees

of freedom. Among the studied models, the compact model based on neural network is the best algorithm to describe the specific resistance with a MSE lower than  $1.44 \times 10^{-12} \Omega cm^2$ . Additionally, the neural network can be used for systems with more than three degrees of freedom.

In this manuscript, the ballistic resistivity due to the grain boundary effect has been studied. While electron phonon scattering are reported to play an important role in copper resistivity at room temperature and when the grains are larger [2, 33], these effects have not been included in this work. Future work will use the neural network to generate a compact model that includes electron-phonon scattering in addition to grain boundary effects to describe the resistivity for copper interconnects.

## ACKNOWLEDGMENTS

This work was supported by the FAME Center, one of six centres of STARnet, a Semiconductor Research Corporation program sponsored by MARCO and DARPA. Support by the US Department of Energy National Nuclear Security Administration under Grant No. DE-FC52-08NA28617 is acknowledged. The authors also acknowledge the staff and computing resources of both the Rosen Center for Advanced Computing (RCAC) at Purdue University and the Blue Waters sustained-petascale computing project, which is supported by the National Science Foundation (award number ACI 1238993). Finally, the authors would like to thank Dr. Bozidar Novakovic and David Guzman for stimulating discussions about the topic.

### A. Appendix

Parameters for bulk copper with the environmental tight binding method (TB) are obtained by direct fitting bulk band structure [10], but additional constraints on the interatomic coupling are included during the parametrization process.

Parameter Name	Value	Parameter Name	Value
<i>VBO</i>	3.6540	<i>I_D_D_Δ</i>	-0.08
<i>E_S</i>	-4.5236	<i>q_D_D_σ</i>	4.8355
<i>E_Px</i>	-0.1458	<i>q_D_D_Π</i>	4.7528
<i>E_Py</i>	-0.1458	<i>q_D_D_Δ</i>	4.2950
<i>E_Pz</i>	-0.1458	<i>I_S_S_σ</i>	0.4
<i>E_Dxy</i>	-4.3034	<i>I_S_P_σ</i>	0.4457
<i>E_Dyz</i>	-4.3034	<i>I_S_D_σ</i>	-0.36819
<i>E_Dxz</i>	-4.3034	<i>I_P_P_σ</i>	1.5605
<i>E_Dz<sup>2</sup></i>	-4.3034	<i>I_P_D_σ</i>	-0.2532
<i>E_Dx<sup>2</sup>_y<sup>2</sup></i>	-4.3034	<i>I_P_P_Π</i>	-0.1348
<i>V_S_S_σ</i>	-0.9588	<i>I_P_D_Π</i>	0.0135
<i>V_S_P_σ</i>	1.4063	<i>q_S_S_σ</i>	2.20333
<i>V_S_D_σ</i>	-0.1841	<i>q_S_P_σ</i>	2.6554
<i>V_P_P_σ</i>	1.4025	<i>q_S_D_σ</i>	0.2495
<i>V_P_P_Π</i>	-0.5730	<i>q_P_P_σ</i>	1.5905
<i>V_P_D_σ</i>	-0.4607	<i>q_P_P_Π</i>	2.9059
<i>V_P_D_Π</i>	0.3373	<i>q_P_D_σ</i>	3.8124
<i>V_D_D_σ</i>	-0.3709	<i>q_P_D_Π</i>	3.9330
<i>V_D_D_Π</i>	0.2760	<i>p_S_S_σ</i>	1.3692
<i>V_D_D_Δ</i>	-0.0735	<i>p_S_P_σ</i>	2.8794
<i>I_D_D_σ</i>	-0.15	<i>p_S_D_σ</i>	3.94296
<i>I_D_D_Π</i>	-0.2498	<i>p_P_P_σ</i>	5.5023
<i>p_P_P_Π</i>	0.536231	<i>p_P_D_σ</i>	-1
<i>p_P_D_Π</i>	-1	<i>p_D_D_σ</i>	-0.83723
<i>p_D_D_Π</i>	0.66507	<i>p_D_D_Δ</i>	4.8475
<i>R<sub>0</sub>-inter</i>	0.25526	<i>R<sub>0</sub>-intra</i>	0.25526

TABLE II. TB parameters for Cu following the notation on ref [10]

- 
- [1] “International roadmap for semiconductors, <http://public.itrs.net/reports.html>,” (2014).
- [2] R. L. Graham, G. B. Alers, T. Mountsier, N. Shamma, S. Dhuey, S. Cabrini, R. H. Geiss, D. T. Read, and S. Peddeti, *Applied Physics Letters* **96**, 042116 (2010).
- [3] K. Fuchs and N. F. Mott, *Mathematical Proceedings of the Cambridge Philosophical Society* **34**, 100 (1938).
- [4] A. F. Mayadas, *Applied Physics Letters* **14**, 345 (1969).
- [5] M. César, D. Liu, D. Gall, and H. Guo, *Physical Review Applied* **2**, 044007 (2014).
- [6] T.-H. Kim, X.-G. Zhang, D. M. Nicholson, B. M. Evans, N. S. Kulkarni, B. Radhakrishnan, E. A. Kenik, and A.-P. Li, *Nano letters* **10**, 3096 (2010).

- [7] B. Feldman, S. Park, M. Haverty, S. Shankar, and S. T. Dunham, *physica status solidi (b)* **247**, 1791 (2010).
- [8] B. Zhou, Y. Xu, S. Wang, G. Zhou, and K. Xia, *Solid State Communications* **150**, 1422 (2010).
- [9] X.-G. Zhang, K. Varga, and S. T. Pantelides, *Physical Review B* **76**, 035108 (2007).
- [10] G. Hegde, M. Povolotskyi, T. Kubis, T. Boykin, and G. Klimeck, *Journal of Applied Physics* **115**, 123703 (2014).
- [11] R. Hoffmann, *Reviews of Modern Physics* **60**, 601 (1988).
- [12] J. Cerdá and F. Soria, *Physical Review B* **61**, 7965 (2000).
- [13] M. Brandbyge, J.-L. Mozos, P. Ordejón, J. Taylor, and K. Stokbro, *Physical Review B* **65**, 165401 (2002).
- [14] M. E. Straumanis, L. S. Yu, and IUCr, *Acta Crystallographica Section A* **25**, 676 (1969).
- [15] P. D. Bristowe and A. G. Crocker, *Philosophical Magazine A* **38**, 487 (1978).
- [16] GBStudio, “<https://staff.aist.go.jp/h.ogawa/GBstudio/indexE.html>,” (2014).
- [17] R. Lake, G. Klimeck, R. C. Bowen, and D. Jovanovic, *Journal of Applied Physics* **81**, 7845 (1997).
- [18] S. Steiger, M. Povolotskyi, H.-H. Park, T. Kubis, and G. Klimeck, “NEMO5: A Parallel Multiscale Nanoelectronics Modeling Tool,” (2011).
- [19] Supriyo Datta, *Electronic transport in mesoscopic systems* (Cambridge University Press, Cambridge, 1997).
- [20] D. Valencia, E. Wilson, P. Sarangapani, G. A. Valencia-Zapata, G. Klimeck, M. Povolotskyi, and Z. Jiang, in *2016 International Conference on Simulation of Semiconductor Processes and Devices (SISPAD)* (IEEE, 2016) pp. 105–108.
- [21] L. Lu, Y. Shen, X. Chen, L. Qian, and K. Lu, *Science* **304** (2004).
- [22] S. Plimpton, *Journal of Computational Physics* **117**, 1 (1995).
- [23] Y. Mishin, M. J. Mehl, D. A. Papaconstantopoulos, A. F. Voter, and J. D. Kress, *Physical Review B* **63**, 224106 (2001).
- [24] G. Kresse and J. Furthmüller, *Computational Materials Science* **6**, 15 (1996).
- [25] C. H. Rycroft, G. S. Grest, J. W. Landry, and M. Z. Bazant, *Physical Review E* **74**, 021306 (2006).
- [26] W. J. Conover, *Practical Nonparametric Statistics*, 3rd ed. (Wiley Publication, 1999).

- [27] MATLAB, “Optimization toolbox r2015a,” (2015), the MathWorks, Natick, MA, USA.
- [28] M. Hagan, H. Demuth, and M. Beale, *Neural network design* (PWS Publishing Company, 1996) p. 734.
- [29] L. R. Marim, M. R. Lemes, and A. Dal Pino, *Phys. Rev. A* **67**, 033203 (2003).
- [30] A. Bholoa, S. Kenny, and R. Smith, *Nuclear Instruments and Methods in Physics Research Section B: Beam Interactions with Materials and Atoms* **255**, 1 (2007).
- [31] S. Fritsch, F. Guenther, and M. Suling, *neuralnet: Training of Neural Networks* (R Foundation for Statistical Computing, 2008).
- [32] S. Haykin, *Neural networks-A comprehensive foundation*, 2nd ed. (Prentice Hall, 1999).
- [33] J. J. Plombon, E. Andideh, V. M. Dubin, and J. Maiz, *Applied Physics Letters* **89**, 113124 (2006).